Journal of New Materials for Electrochemical Systems 16, 183-188 (2013)

Understanding the Surface State and Proton Adsorption Phenomena on Ni-based Alloys at the Hydrogen Evolution Zone in Alkaline Medium by EIS-XPS

Miguel A. Oliver-Tolentino[1], Roman Cabrera-Sierra[2], Luis Lartundo-Rojas[3], J. Lucero-Guerrero[4], R. Sotelo-Boyas[4] and Arturo Manzo-Robledo[4,*]

[1]UPIBI-IPN, Departamento de Ciencias Básicas. Av. Acueducto s/n, Barrio La Laguna, Col. Ticomán, México, D.F. 07340, Mexico
[2]ESIQIE-IPN, Departamento de Ingeniería Química-Laboratorio de Química Analítica.
Edif. Z-5 1er piso, UPALM, México D.F. 07738, Mexico
[3]Centro de Nanociencias y Micro y Nanotecnología (CNMN). Luis Enrique Erro s/n, UPALM,
Col. Zacatenco, Mexico D.F. 07738, Mexico
[4]ESIQIE-IPN, Departamento de Ingeniería Química - Laboratorio de Electroquímica y Corrosión.
Edif. Z-5 3er piso, UPALM, Mexico D.F. 07738, Mexico

Received: November 01, 2012, Accepted: January 07, 2013, Available online: July 08, 2013

Abstract: *In this work, well-defined Ni-based alloys, labeled M1 ($Ni_{0.8}CoO_{0.1}Zn_{0.05}MnO_{0.02}Ti_{0.01}Y_{0.01}Al_{0.01}$) and M2 ($NiO_{0.8}CoO_{0.1}Zn_{0.05}MnO_{0.02}Ti_{0.01}Y_{0.01}Al_{0.01}$), were prepared by ball-milling technique and used as electrodes for the generation of hydrogen. Electrochemical Impedance Spectroscopy (EIS) and X-ray photoelectron spectroscopy (XPS) were employed in order to understand the surface state and proton adsorption phenomena during cathodic polarization. It was found that high concentration species such as NiO and/or $Ni(OH)_2$ induces passivation effect, suppressing the HER by increasing the electrode resistance. The charge transfer, double layer capacitance and adsorption of protons toward the electrode interface ware found to be highly controlled by the intrinsic nature of the alloy in turn.*

Keywords: proton adsorption, mechanical milling, electrocatalysis, passivation, metal hydrides.

1. INTRODUCTION

Hydrogen is considered as a promising fuel with regards to environment compatibility, high energy content, versatility, efficiency and cost effectiveness when compared to oil, gasoline, methane, methanol and liquefied-petroleum gas [1, 2]. Hydrogen can be produced via water electrolysis with high yield and purity. Although the hydrogen evolution reaction (HER) has been extensively investigated since the last century [3, 4], interest in finding lower cost electrocatalysts with higher efficiency, compared with noble metals, and stability has been growing tremendously in recent years.

Nickel and its alloys with Co [5], Mo [6], W [7] and Fe [8], as well as Raney-type Ni-Zn-P [9] are promising candidates to promote hydrogen evolution reaction showing satisfactory electrocatalytic activity and stability [4], and sufficient corrosion resistance in alkaline conditions [10].

In particular, Mechanical alloying (MA) method has received significant attention. The MA process has been applied widely in binary and ternary systems, enabling to obtain intermetallic compounds, supersaturated solid solutions and also amorphous alloys [11]. These alloys have the characteristic of forming nanostructures, which are expected to exhibit better physicochemical properties [12].

In a previous work, the electrocatalytic performance of Nickel-based alloys has been studied in the HER region using Tafel analysis [13]. The results in this work indicated that the material labeled M2 exhibited the highest catalytic activity followed by sample M1 and M3, differences linked to corrosion inhibition and alloy-electronic modifications. In this context, techniques such as hydrogen adsorption, Electrochemical Impedance Spectroscopy (EIS)

*To whom correspondence should be addressed: Email: amanzor@ipn.mx
Phone: +52 5557296000, ext. 54246; fax: +52 5555862728

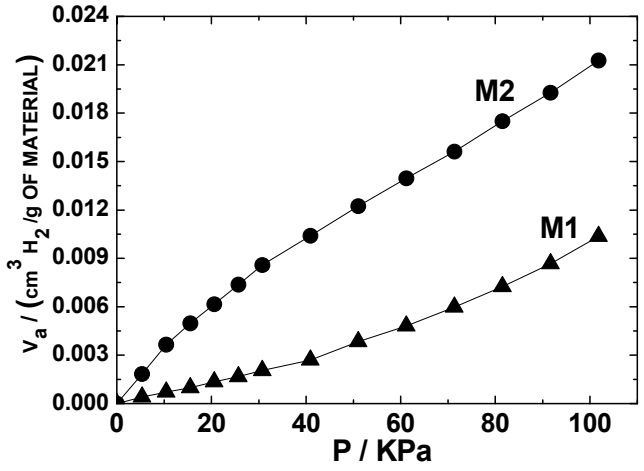

Figure 1. Adsorption isotherms of hydrogen.

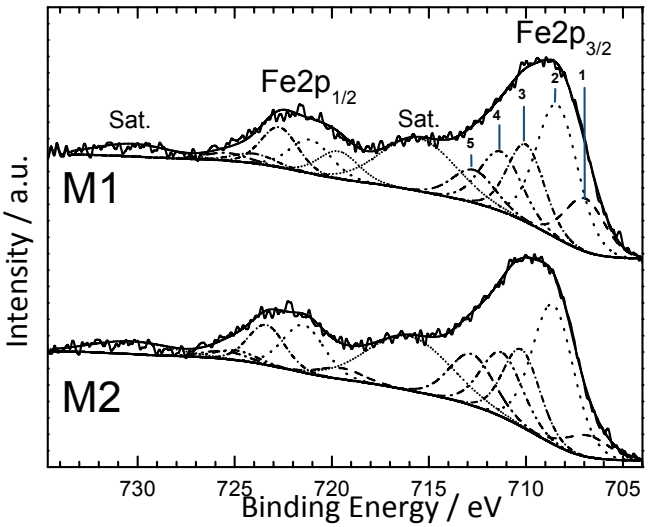

Figure 2. Fe2p region spectrum of samples M1 and M2. The spectrum is fitted with the main $Fe2p_{3/2}$ and $Fe2p_{1/2}$ peaks and the set of Fe species; Fe^{o} (1), FeO (2), Fe_2O_3 (3), FeOOH (4) and Fe/Ni (5).

and X-ray photoelectron spectroscopy (XPS) were employed to better understand the surface effect-interaction during cathodic polarization on samples M1 and M2 (as a multi-metallic alloys), which presented the highest activity toward hydrogen evolution reaction compared with sample M3 with composition $NiO_{0.6}CoO_{0.35}Zn_{0.025}Ti_{0.025}$.

2. EXPERIMENTAL

2.1. Synthesis of Materials

In this work materials such as $Ni_{0.8}CoO_{0.1}Zn_{0.05}MnO_{0.02}Ti_{0.01}Y_{0.01}Al_{0.01}$, and $NiO_{0.8}CoO_{0.1}Zn_{0.05}MnO_{0.02}Ti_{0.01}Y_{0.01}Al_{0.01}$ labeled as M1 and M2 respectively, were obtained from high-energy mechanical milling, using 5.6 g of Ni metallic powder or 5.6 g of NiO for M1 and M2 respectively and mixed with 0.7 g of CoO, 0.35 g of Zn metallic powder, 0.14 g of MnO, 0.07 g of Ti metallic powder, 0.07 g of Y metallic powder and 0.07 g of Al metallic powder. A total amount of 7 g of the powder mixtures and 6 hardened steel balls of 12.7 mm in diameter were loaded into a steel vial; the mechanical alloying process was carried out at room temperature in an air atmosphere using a shaker mixer/mill machine. The ball-to-powder weight ratio was 7:1. To prevent excessive overheating of the vials, all experiments were carried out by means of cycles of 60 min of milling and 15 min off. The milling time tested was 5 h.

2.2. Hydrogen Adsorption

H_2 adsorption experiments at 77K were carried out on samples outgassed at 280ºC (10−4 Pa), with a Micromeritics ASAP 2000 instrument.

2.3. X-ray Photoelectron Spectroscopy

X-ray photoelectron spectroscopic (XPS) analyses were performed using a Thermo Scientific K-Alpha X-ray photoelectron spectrometer with a monochromatized Al*K*a X-ray source (1487 eV) and a base pressure of $1x10^{-9}$ Torr in the analytical chamber. The position of the O1s peak at 531.0 eV was monitored on each sample to ensure that no binding energy shift due to charging had occurred. Survey scans were recorded using 400 mm spot size and fixed pass energy of 160 eV, whereas narrow scans were collected at 60 eV analyzer pass energy. The specimens were nonconductive powders of the as-prepared materials. All of the specimens ware embedded in a 5x5 mm indium foil prior to analysis. Collected XPS spectra were analyzed using Avantage v5.41 from Thermo Fisher Scientific.

2.4. Working Electrode Preparation

The as-prepared materials were deposited on a previously polished surface (5 mm diameter) of a glassy carbon substrate (GC). The inks were prepared using 5 mg of the alloy in turn, 6 µL Nafion (5wt %, Aldrich) and 60 mL of ethanol. The suspension was homogenized by ultrasound. Sample deposits onto the GC substrate were done with an aliquot of 5 µL of the ink, and then dried in atmosphere of argon for 5 min.

2.5. Electrochemical Measurements

A three-electrode standard electrochemical cell was employed. A carbon rod and a Calomel (SCE) electrode were used as counter and reference electrodes, respectively. Prior to use, the solution was purged with argon for at least 15 min. The EIS experiments were recorded at open circuit potential (OCP), -1.0, -1.1 and -1.2 V/SCE using amplitude of 10 mV and a frequency scan from 10 kHz to 10 mHz, in a Potentiostat/Galvanostat (VersaSTAT 3-200). A 5M NaOH solution was used as supporting electrolyte. The electrochemical experiments were performed at a rotation speed of 1000 rpm.

3. RESULTS AND DISCUSSION

3.1. Hydrogen adsorption

In Figure 1 it is possible to observe the hydrogen-adsorption isotherms obtained from 0 to 101 KPa for the samples in study. These profiles put in evidence that the maximum hydrogen uptake is 0.001 and 0.02 cm^3 / g for M1 and M2, respectively. The latter

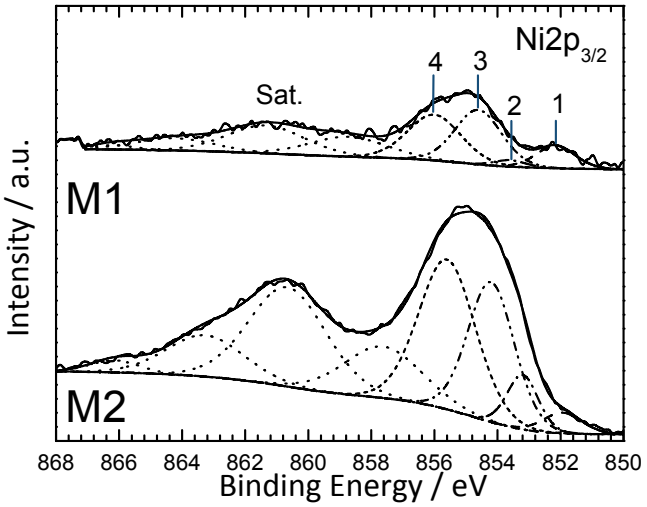

Figure 3. Ni2p region spectrum of samples M1 and M2. The spectrum is fitted with the main Fe2p3/2 peak and the set of Fe species; Ni (1), NiO (2), $Ni(OH)_2$ (3), NiOOH(4) and the set of satellites associated to Ni, NiO and Ni(OH).

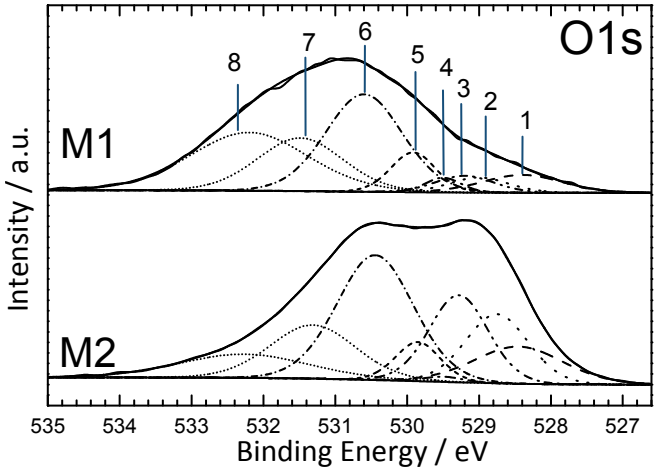

Figure 4. O1s region spectrum of samples M1 and M2. The spectrum is fitted with the main O1s peak and the set of species; Oxi species (1), NiO (2), CoO (3), Fe_2O_3 (4), MnO (5), TiO_2, ZnO (6) and finally adsorbed OH^- (7) and H_2O (8).

result indicates that M2-hydrogen adsorption capacity is higher than that for sample M1, as it is discussed in the next sections.

3.2. X-ray Photon Spectroscopy analysis

The presence of Ni, Co, Zn, Mn, Ti, Y, Al, and O has been confirmed by XPS in both samples. Although iron was also observed due to contamination from balls and container. On the other hand, chemical species associated with Zn, Co, Mn, Ti, Y and Al did not present important differences in both samples. However nickel, iron and oxygen exhibited interesting differences between M1 and M2. For example, Figure 2 shows Fe2p high-resolution XPS spectrum for samples M1 and M2. In the case of sample M1 Fe-oxidation state (0), in both main $Fe2p_{3/2}$ and $Fe2p_{1/2}$ peaks, is observed at a binding energies (BE) of 707.61 eV and 720.31 eV respectively. Whereas in M2, Fe^0 appears near to 708.06 eV and at 720.76 eV [14]. In addition, for both samples, the signals associated to FeO specie are located at BE of 709.5 eV, $Fe2P_{3/2}$ peak, and near to 722 eV, $Fe2P_{1/2}$ peak [15]. Finally, $Fe2p_{3/2}$ and $Fe2p_{1/2}$ contributions related to Fe^{3+} in Fe_2O_3 are located at 711.14 (710.97) eV at 723.84 (723.67) eV for M1 (M2).

This shift suggests the presence of two different Fe_2O_3-phases: γ for M2 and α for M1. Therefore, the main difference between the two sets of samples is the coordination of the Fe^{3+} cations. That is, in the α-compounds, the crystal structure is oriented in such a way that all of the cations are octahedrally coordinated [16]. Nevertheless, in the γ-compounds three-quarters of the Fe^{3+} cations are octahedrally coordinated whereas the other quarter of the cations is tetrahedrally coordinated [17]. Then cation vacancies are presented in the crystal structure of the γ-compounds to balance the overall charge. Also in Figure 2, the peak at a BE of 712 eV (Fe2p1/2 contribution near to 724.5 eV) is associated to the presence of α-FeOOH and γ-FeOOH which is overlapped with the signal attributed to Fe-Ni interactions, probably from $FeNi_3$ phase [13]. The signal around 716 eV can be assigned to $Fe2p_{3/2}$ shake-up satellites.

Following this analysis, Ni2p region XPS spectrum (Figure 3) denotes, at 852 eV, the contribution associated to metallic nickel with its corresponding satellite at a BE of 858 eV. The contribution attributed to NiO is observed at 853 eV, with its two satellites positioned at 861 and 864 eV. Near to 854 eV it is found the contributions of $Ni(OH)_2$ with its satellite at 866 eV. Around 856eV it is evident the band associated to NiOOH in both phases γ and β [17,18].

Lastly, the high resolutions XPS spectrum for oxygen (O1s) is shown in Figure 4. It is clear that at the range from 527 to 529.5 eV, which is associated to O^{2-}-oxi species, sample M2 exhibits more intense peak contributions with respect to M1. At this region, the presence of NiO, BE of 528.75 eV, and CoO, at 529.28 eV, was evinced. The small signal at 529.5 eV might be attributed to iron-oxo species with oxidation state of Fe^{3+}, the MnO is observed around 529.85 eV. Conversely, the peak at 530.44 eV indicates the presences of TiO_2-ZnO mixture. The adsorbed species OH^- and H_2O can be found at 531.31 and 532.27 eV, respectively.

The surface-spectral fitting parameters corresponding to M1 and M2 obtained by XPS data, are reported in Table 1. These results revealed that M2 presents a major quantity of FeOOH, O^{2-}, NiOOH and NiO species, compared with M1. In addition, M1 presents, in percentage, a greater amount of metallic nickel than its counterpart as Ni^0 was employed for the synthesis.

3.3. Electrochemical Impedance Spectroscopy

Impedance diagrams obtained at open circuit potential ($E_{i=0}$), -1.0, -1.1 and -1.2 V/SCE are observed in Figure 5 for M1 and M2. In these experiments the electrode was immersed in a 5M solution of NaOH. Significant differences were detected mainly in the complex plane. In this context, both samples generate a capacitive response; however, the impedance values are higher at M1 compared with M2, suggesting a more resistive behavior at the interface of M1. Therefore, taking in to account the results obtained by XPS, conduction-intrinsic properties in both materials are highly associa-

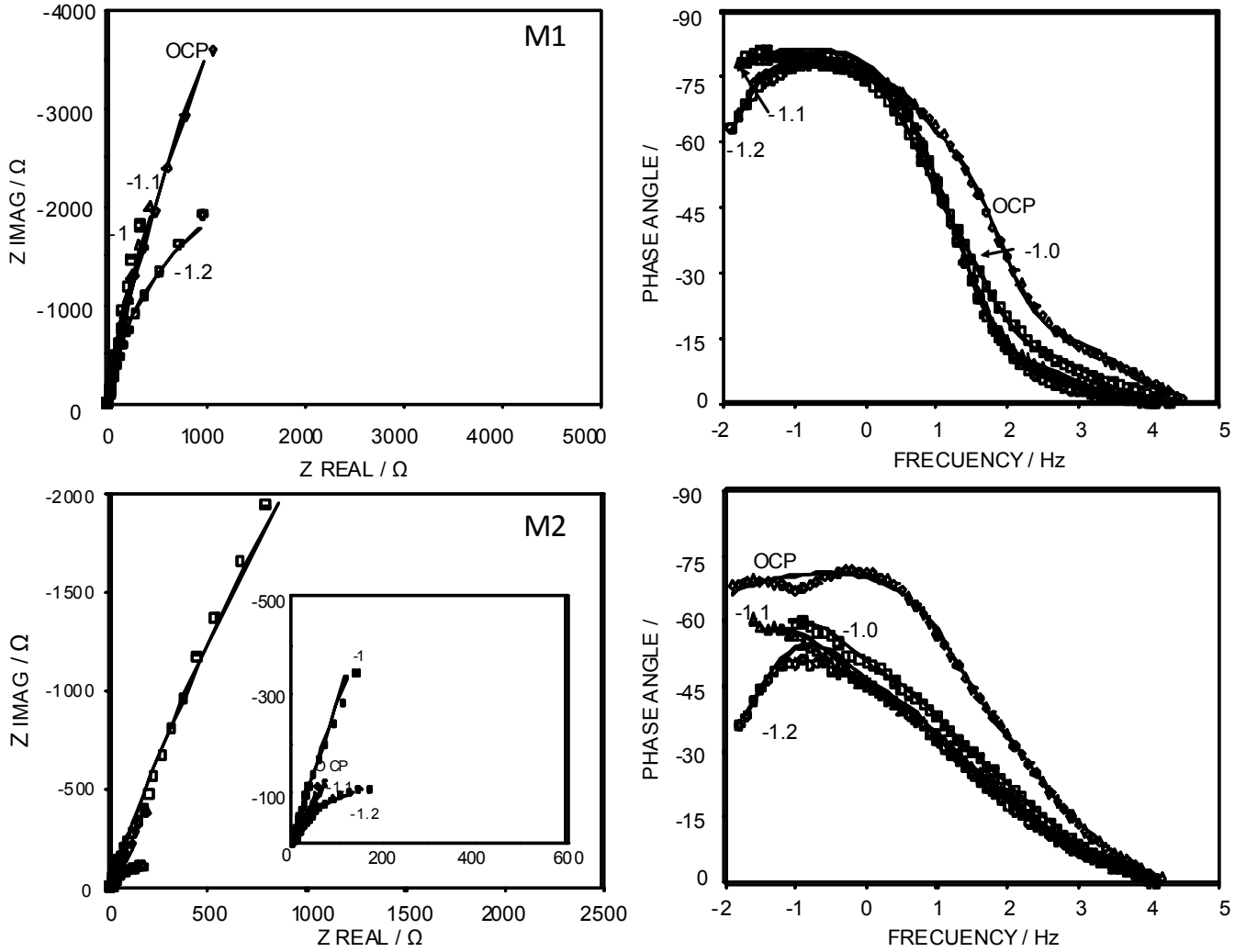

Figure 5. Impedance diagrams obtained for M1 and M2 at OCP, -1, -1.1 and -1.2 V, immersed in 5M NaOH.

Table 1. Surface stoichiometry for samples M1 and M2 obtained by the X-ray Photoelectron Spectroscopy (XPS).

Fe (at%)						
Sample	Fe %	FeO %	Fe_2O_3 %	FeOOH %	Fe/Ni %	Total Fe
M1	16.85	36.43	22.60	15.09	9.03	100
M2	7.36	40.44	22.45	16.00	13.74	100

Ni (at%)									
Sample	Ni^0%	NiO %	$Ni(OH)_2$ %	NiOOH %	Ni sat %	NiO sat %	NiO sat2 %	$Ni(OH)_2$ sat %	Total Ni
M1	8.04	1.88	23.31	22.46	14.10	19.78	8.73	1.71	100.00
M2	2.42	5.14	19.75	25.81	12.09	23.30	9.70	1.80	100.00

O_2 (at%)									
Sample	O^{2-}%	NiO %	CoO %	Fe_2O_3 %	MnO%	TiO_2, ZnO%	OH^- %	H_2O ads%	Total O_2 %
M1	5.81	3.65	4.00	2.13	7.27	30.60	18.57	27.99	100.00
M2	10.36	13.57	16.05	0.63	5.47	30.00	14.35	9.57	100.00

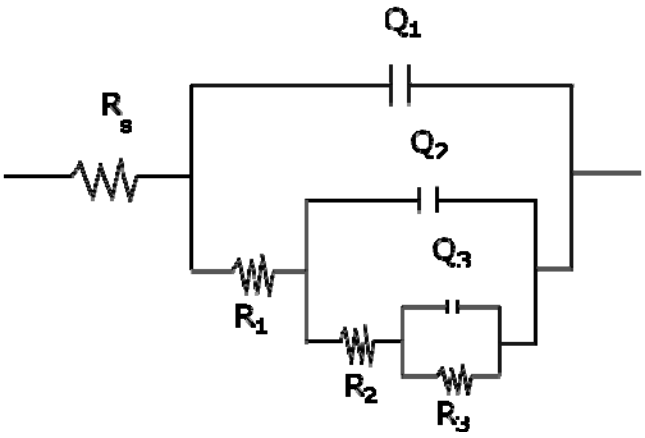

Figure 6. Equivalent circuit used for fitting the EIS experimental data obtained for M1 and M2 immersed in 5 M NaOH.

ted with surface-species, especially those linked with nickel. These properties give at M2 the better catalytic activity for HER. As a manner to confirm this assumption, the Bode diagrams indicated an apparent formation of a capacitive maximum at low and intermediate frequencies, with angle values different from zero in the high frequency region. The material M2 exhibited the lower angle values. Moreover, at lower angle values an irregular response is observed as potential becomes more negative. This low-noise signal is associated with the reduction of water and the formation of molecular hydrogen at the electrode surface.

The experimental data from Figure 5 were modeled using Boukamp software using the electrical equivalent circuit showed in Figure 6. This equivalent circuit considers the presence of three simultaneous steps linked to the electrochemical reduction of water to form hydrogen. In Figure 6, the elements (R_1-Q_1) are associated with the charge transfer resistance and double layer capacitance, (R_2-Q_2) are assigned with the resistance related to the hydrogen adsorption, usually called the pseudo-resistance, and (R_3-Q_3) is related to a passive condition of the Ni supported on M1 and M2. It is important to mention that in this analysis a Constant Phase Elements instead of Capacitance elements was used, due to inherent irregularities in our materials as supported in the glassy carbon electrode. Simulated data results are observed by solid line in Figure 5 and the parameters obtained are shown in Tables 2 and 3.

The electric parameters obtained from simulation are in the same order of magnitude for both materials. However, the value of capacitance and resistive element (R_3) are different. The resistive parameter associated with the solution resistance (Rs) changes as a function of applied potential in the same order of magnitude, due to the ionic resistance of the electrolyte.

On the other hand, the associated pseudo-capacitance for M1 and M2 were obtained using constant-phase element parameters Q_1 (Y_o and n) and the expression $C = ((Y_{o1} \times R_1)^{1/n})/R_1$ [19]. This capacitive contribution linked to dielectric properties is different. For example, in M1 the capacitance increases with the applied potential, whereas in M2 the values are one order of magnitude higher, indicating that the conductive properties for M2 are also higher as compared to M1. This behavior can be associated to the presence of γ and β-NiOOH, which promotes the formation of NiH [20].

The difference in magnitude of the element R_1 (M1<M2), which is associated to charge transfer, can be attributed to the presence of metallic Ni, which is presented in a greater amount at sample M1, suggesting that water reduction occurs on Ni-metallic sites.

However, the element R_2 (related to the hydrogen adsorption) is in the order M2>M1, indicating that in sample M2 the diffusion of protons is more efficient, due to heterogeneity, roughness, particle size and its higher porosity, as confirmed by SEM [13]. Although mores studies are necessary, the element R2 might be also associated with the γ-FeOOH species and cation vacancies in the crystal structure.

On the other hand, the contribution of R3 has important conse-

Table 2. Parameters obtained by fitting the EIS diagrams of M1 using the equivalent circuit shown in Figure 6 and Boukamp program.

E	R_s	Q_1		C	R_1	Q_2		R_2	Q_3		R_3
	(Ω)	Y_0 ($\times 10^4 \Omega.s^n$)	n	(μF)	(Ω)	Y_0 ($\times 10^4 \Omega.s^n$)	n	(Ω)	Y_0 ($\times 10^4 \Omega.s^n$)	n	(Ω)
OCP	2.9	2.88	0.86	89.5	2.2	7.76	0.89	67.9	3.25	0.89	38628
-1.0	2.8	7.72	0.88	307.1	1.5	16.0	0.92	13.3	14.2	0.90	23706
-1.1	2.8	10.1	0.92	550.9	0.93	24.9	0.93	22.2	7.37	0.90	17991
-1.2	2.7	14.4	0.94	923.6	0.66	25.5	0.93	42.8	7.0	0.90	54449

Table 3. Parameters obtained by fitting the EIS diagrams of M2 using the equivalent circuit shown in Figure 6 and Boukamp program.

E	R_s	Q_1		C	R_1	Q_2		R_2	Q_3		R_3
	(Ω)	Y_0 ($\times 10^4 \Omega.s^n$)	n	(μF)	(Ω)	Y_0 ($\times 10^4 \Omega.s^n$)	n	(Ω)	Y_0 ($\times 10^4 \Omega.s^n$)	n	(Ω)
OCP	1.77	75.9	0.67	1616.1	5.7	51.8	0.74	67.03	31.4	0.89	1633.9
-1.0	1.81	2.06	1.0	206.0	1.1	3.53	1.0	3.07	28.8	0.76	26627
-1.1	1.8	87.9	0.66	1566.7	4.0	73.5	0.72	34.4	81.0	0.81	1356.0
-1.2	1.81	68.7	0.71	1407.2	3.0	86.5	0.77	29.1	93.0	0.85	252.3

quences as it includes electrode-passivation phenomenon at the vicinity of nickel-sites [2] induced by the solution-pH (e.g. alkaline), and promoting the precipitation of nickel compounds, such as NiO and/or $Ni(OH)_2$, which were identified by XPS in this study. In this context, the major nickel-compounds concentration was found at sample M1, as a consequence the value of R3 is in the order M1>M2, see Tables 2 and 3. As passivation phenomena are more facile-induced at M1 surface, the HER is suppressed by increasing the electrode resistance.

4. CONCLUSION

Metallic alloys based on nickel were evaluated in the cathodic region in order to induce the proton-adsorption and hydrogen-evolution reaction. It was found that such a reaction is controlled by the species-nature present at the alloy in turn as demonstrated by XPS analysis. For sample M1 the presence of NiO and/or $Ni(OH)_2$ induces a passivation phenomena, decreasing its activity for HER. Conversely, for sample M2, the presence of γ and β-NiOOH and γ-FeOOH species, as well as crystal structure orientation and cation vacancies in the crystal structure, promote the formation of metal hydrides and, eventually the HER, as conduction properties become more efficient with the applied potential.

5. ACKNOWLEDGMENTS

The authors thank the financial support through projects of SIP-ESIQIE-IPN 20120499 and CONACyT (160333).

REFERENCES

[1] T.N. Veziroglu, F. Barbir, Int. J. Hydrogen Energy, 17, 391 (1992).
[2] W. Lubitz, W. Tumas, Chem. Rev., 107, 3900 (2007).
[3] B.E. Conway, L. Bai, J. Electroanal. Chem., 198, 149 (1986).
[4] Y. Choquette, L. Brossard, A. Lasia, H. Menard, J. Electrochem. Soc., 137, 1723 (1990).
[5] M.J. de Giz, S.A.S. Machado, L.A. Avaca, E.R. Gonzalez, J. Appl. Electrochem., 22, 973 (1992).
[6] B.E. Conway, L. Bai, J. Chem. Soc., Faraday Trans., 1, 1841 (1985).
[7] M.A. Oliver-Tolentino, E.M. Arce-Estrada, C.A. Cortés-Escobedo, A.M. Bolarín-Miro, F. Sánchez de Jesús, R.G. González-Huerta, A. Manzo-Robledo, J. Alloys Comp., 536, 245 (2012).
[8] J. de Carvalho, G. Filho Tremiliosi, L.A. Avaca, E.R. Gonzalez, Int. J. Hydrogen Energy, 14, 161 (1989).
[9] R.K. Shervedani, A. Lasia, J. Electrochem. Soc., 144, 511 (1997).
[10] F. Rosalbino, S. Delsante, G. Borzone, E. Angeline, Int. J. Hydrogen Energy, 33, 6696 (2008).
[11] Koch CC. In: Cahn RW, Haasen P, Kramer ES, editors. Mat. Sci. and Tech., vol. 15. Weinheim: VCH; 1991. p.583.
[12] M.A. Domínguez-Crespo, M. Plata-Torres, A.M. Torres-Huerta, I.A. Ortiz-Rodríguez, C. Ramírez-Rodríguez, E.M. Arce-Estrada, Mater. Charact., 56, 138 (2006).
[13] L. Vázquez-Nava, K. Patlán-Olmedo, M.A. Oliver-Tolentino, R. González-Huerta, H.J. Dorante-Rosales, A. Guzmán-Vargas, A. Manzo-Robledo, J. New Mat. Electrochem. Systems, 15, 211 (2012).
[14] M.C. Biesinger, B.P. Payne, A.P. Grosvenor, L.M.W. Lau, A.R. Gerson, R.St.C. Smart, Appl. Surf. Sci., 257, 2717 (2011).
[15] M. Descostes, F. Mercier, N. Thromat, C. Beaucaire, M. Gautier-Soyer, Appl. Surf. Sci., 165, 288 (2000).
[16] M. Moukassi, M. Gougeon, P. Steinmetz, B. Dupre, C. Gleitzer, Metall. Trans. B, 15, 383 (1984).
[17] A.P. Grosvenor, B.A. Kobe, M.C. Biesinger, N.S. McIntyre, Surf. Interface Anal., 36, 1564 (2004).
[18] A.P. Grosvenor, M.C. Biesinger, R.St.C. Smart, N.S. McIntyre, Surf. Sci., 600, 1771 (2006).
[19] M.A. Pech Canul, L.P. Chi Canul, Corrosion, 55, 948 (1999).
[20] J. Vazquez-Arenas, L. Altamirano-Garcia, T. Treeratanaphitak, M. Pritzker, R. Luna-Sanchez, R. Cabrera-sierra, Electrochimica Acta, 65, 234 (2012).